Cell, Vol. 91, 741–752, December 12, 1997, Copyright ©1997 by Cell Press

Solution Structure of the KIX Domain of CBP Bound to the Transactivation Domain of CREB: A Model for Activator:Coactivator Interactions

Ishwar Radhakrishnan,* Gabriela C. Pérez-Alvarado,* David Parker,† H. Jane Dyson,* Marc R. Montminy,† and Peter E. Wright*‡
*Department of Molecular Biology
and The Skaggs Institute for Chemical Biology
The Scripps Research Institute
10550 N. Torrey Pines Road
La Jolla, California 92037
†Research Division
Joslin Diabetes Center
Department of Cell Biology
Harvard Medical School
Boston, Massachusetts 02215

Summary

The nuclear factor CREB activates transcription of target genes in part through direct interactions with the KIX domain of the coactivator CBP in a phosphorylation-dependent manner. The solution structure of the complex formed by the phosphorylated kinase-inducible domain (pKID) of CREB with KIX reveals that pKID undergoes a coil→helix folding transition upon binding to KIX, forming two α helices. The amphipathic helix αB of pKID interacts with a hydrophobic groove defined by helices α1 and α3 of KIX. The other pKID helix, αA, contacts a different face of the α3 helix. The phosphate group of the critical phosphoserine residue of pKID forms a hydrogen bond to the side chain of Tyr-658 of KIX. The structure provides a model for interactions between other transactivation domains and their targets.

Introduction

Transcriptional activators are believed to stimulate gene expression via protein–protein interactions with the basal machinery (Ptashne and Gann, 1997). Although certain activators may directly contact the transcriptional apparatus, others require multivalent coactivators to mediate these interactions. The functional importance of such coactivators is clear, but little is known about the structural basis of activator–coactivator recognition.

The cAMP-regulated transcription factor CREB has been shown to stimulate target gene expression, in part by associating with the coactivator paralogs P300 and CREB binding protein (CBP) (Chrivia et al., 1993; Arias et al., 1994; Kwok et al., 1994). Complex formation between CREB and CBP/P300 requires protein kinase A (PKA) mediated phosphorylation of CREB at Ser-133 (Chrivia et al., 1993; Parker et al., 1996). About 50% of cellular CREB protein is Ser-133 phosphorylated in response to a maximal stimulus, and weaker signals induce proportionately lower levels of phosphorylation as well as target gene activation (Hagiwara et al., 1992).

Although phosphorylation has been shown to regulate some transcription factors via their DNA binding or nuclear targeting activities, CREB belongs to a group whose transactivation potential is specifically affected (Gonzalez and Montminy, 1989; Brindle et al., 1993). The CREB transactivation domain is bipartite, consisting of kinase-inducible and constitutive domains termed KID and Q2, respectively, which function synergistically in response to hormonal stimulation (Brindle et al., 1993). The Q2 domain has been shown to stimulate transcription via its association with $hTAF_{II}130$, a subunit of TFIID (Ferreri et al., 1994; Nakajima et al., 1997b). The KID region has been found to regulate target gene expression by interacting with CBP and P300 in a phosphoSer-133- (pSer-133) dependent manner (Parker et al., 1996).

First characterized as coactivators for Ser-133 phosphorylated CREB, CBP and P300 also appear to function as mediators for a number of signal-dependent factors including Jun (Arias et al., 1994), Sap-1a (Janknecht and Nordheim, 1994), STAT-2 (Bhattacharya et al., 1996), as well as certain nuclear receptors (Chakravarti et al., 1996; Kamei et al., 1996). Complex formation with CBP/P300 has been proposed to stimulate chromatin remodeling on target promoters via intrinsic and associated histone acetyltransferase activities (Bannister and Kouzarides, 1996; Ogryzko et al., 1996). Subsequent transcriptional induction is thought to proceed via the CBP/P300-dependent recruitment of RNA polymerase II complexes (Kee et al., 1996; Nakajima et al., 1997a, 1997b).

CBP and P300 bind to the Ser-133-phosphorylated KID region of CREB via a domain referred to as KIX, which is highly conserved in CBP homologs from Caenorhabditis elegans and Drosophila melanogaster (Parker et al., 1996). pSer-133 appears to participate directly in binding to KIX, as revealed by phosphatase protection and cross-linking studies with thio-phosphorylated KID peptides. Hydrophobic interactions also play a role in complex formation since the KID:KIX complex is disrupted by low concentrations of nonionic detergents, and mutation of hydrophobic residues in either KID or KIX severely affects binding (Parker et al., 1996).

In addition to CREB, the KIX domain of CBP also recognizes the transactivation domains of other nuclear factors, including Myb (Dai et al., 1996), Jun (Arias et al., 1994), cubitus interruptus (Akimaru et al., 1997), and HTLV-1 virally encoded Tax protein (Kwok et al., 1996). No consensus KIX-recognition motif has emerged from sequence alignments between these factors. Here we describe the solution structure of KIX complexed to KID phosphorylated at Ser-133. The structure establishes the molecular basis for pKID-KIX recognition and provides insights into the determinants of specificity for complex formation with other activators.

Results and Discussion

Structure Determination

^{1}H-^{15}N-correlated NMR (nuclear magnetic resonance) spectra of the minimal KIX domain of mouse CBP, previously localized to residues 586–679 (Gonzalez et al.,

‡To whom correspondence should be addressed.

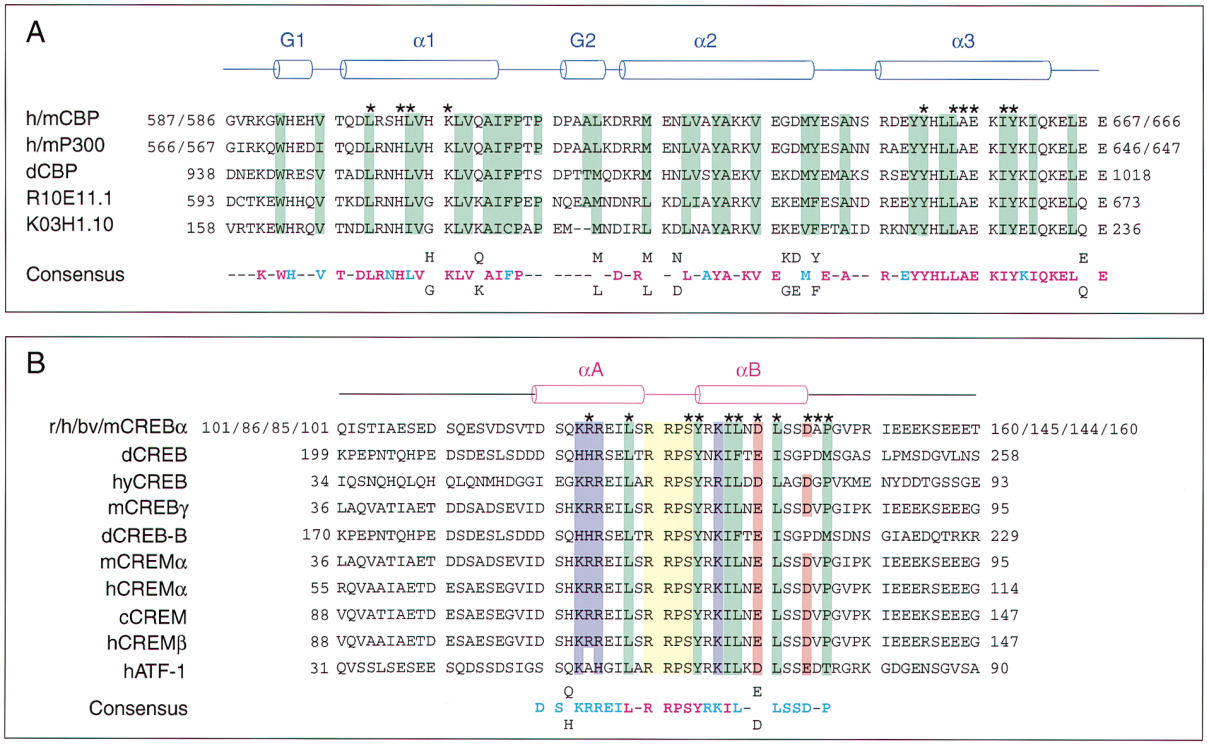

Figure 1. Sequence Alignments of KIX and pKID Domains

Alignments of (A) KIX and (B) pKID domain sequences from various species (prefix abbreviations are: bv, bovine; c, canine; d, Drosophila; h, human; hy, hydra; m, mouse; r, rat). Conserved hydrophobic residues are highlighted in green, and residues involved in contacts between pKID and KIX are indicated by stars. Conserved basic residues in the pKID domain are highlighted in purple, acidic residues in red, and residues that form the invariant phosphorylation motif in yellow. The consensus sequences are color coded as follows: invariant residues (magenta), a position that is invariant in 70% of the cases (cyan), a position always occupied by either one of two residues, in which case both are shown (black). Alignments were performed using the program BLAST (Altschul et al., 1990) for protein sequences in the NCBI database.

1991; Parker et al., 1996), showed signals characteristic of a folded protein plus sharp resonances indicative of an unstructured region. The C terminus was therefore truncated to residue 666 (Figure 1A). This region of CBP and the previously identified KID region (residues 101–160) of rat CREB (Gonzalez et al., 1991) (Figure 1B) were expressed separately in E. coli. GST-fusion proteins bearing these minimal regions of CBP and CREB retain binding affinities similar to those of the full-length proteins in in vitro assays.

The ^{1}H-^{15}N correlated HSQC (heteronuclear single quantum coherence) spectrum of the residue 586–666 minimal KIX construct is well dispersed when complexed to pKID, indicating a unique folded conformation (data not shown). This is in contrast to spectra of the free KIX construct, which aggregates or is unfolded depending on the pH of the solution; this instability appears to be an artifact of the construct, as two longer proteins corresponding to residues 586–672 and 586–679 of mouse CBP appear to be fully folded.

The NMR spectra of free pKID have the characteristics of an unstructured peptide (Figure 2A). Analysis of the $^{1}H^{\alpha}$ chemical shifts and proton–proton NOEs (nuclear Overhauser effects) suggests that the peptide may have a slight propensity toward spontaneous helix formation in the KIX binding region, but the population of helix in free pKID is extremely small. The NH and $^{1}H^{\alpha}$ resonances are sharp and poorly dispersed, and their chemical shifts do not deviate significantly from random coil values. Upon binding to KIX, the resonances of many residues in the region between Ser-121 and Ser-143 are shifted and broadened (Figure 2B), suggesting that a conformational rearrangement accompanies binding. Many of the resonances of residues Arg-130–Tyr-134 are severely broadened in spectra recorded at 42°C but sharpen at lower temperatures, suggesting residual conformational fluctuations in the bound pKID. Both $^{13}C^{\alpha}$ and $^{1}H^{\alpha}$ chemical shifts and the observed pattern of medium range NOEs establish unequivocally that pKID folds to form two helices upon binding to KIX. Even in the KIX complex, residues 101–120 and 146–160 of pKID exhibit resonances that are sharp and have chemical shifts close to random coil values (Figure 2), indicating that these regions remain largely unstructured and flexible.

Solution structures were calculated using interproton distance and torsion angle restraints derived from multidimensional NMR data (Table 1). Only the structured region of pKID, residues 119–146, was included in the calculations; no intermolecular NOEs were observed between KIX and residues of pKID outside this region.

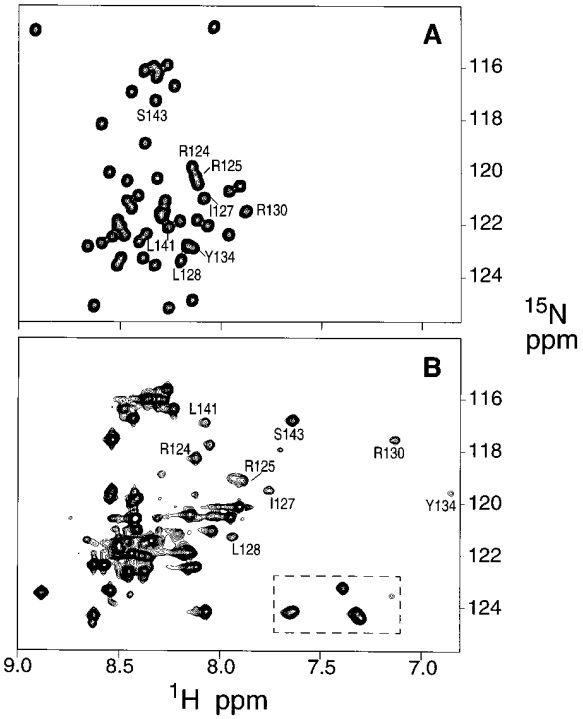

Figure 2. ^{1}H-^{15}N Correlated NMR Spectra of pKID

Regions of the ^{1}H-^{15}N-correlated HSQC spectra of (A) free pKID and (B) pKID bound to the KIX domain. Some of the pKID resonances that are significantly shifted upon complexation with KIX are labeled. The intense, narrow resonances in the region from 7.8 to 8.7 ppm in the pKID:KIX complex arise from residues in the unstructured N-and C-terminal regions of the bound pKID. Arginine side chain resonances are enclosed within the hatched area of (B).

Sixteen structures were selected for analysis (Figure 3); these structures have good backbone conformations and no serious constraint violations (Table 1).

Overall Structure of the Complex

The KIX domain of CBP is composed of three mutually interacting α helices, designated α1, α2 and α3, and two short 3_{10} helices, G1 and G2, that together with the interconnecting loops define a compact structural domain with an extensive hydrophobic core (Figure 3C). Helices α1 and α3 constitute the primary interacting surface for the pKID polypeptide, forming a hydrophobic patch on the protein surface that is large enough to accommodate up to 3 turns of an amphipathic α helix, designated αB, in pKID (Figure 4). A second α helix in pKID, referred to as αA, interacts with a different face of the α3 helix of KIX (Figure 3). The two helices of pKID are arranged at an angle of about 90° and essentially wrap around the α3 helix of KIX.

Structure of the KIX Domain

The KIX domain has a novel fold with no close relatives in the FSSP database of structurally aligned protein fold families (Holm and Sander, 1994). Helix α1 encompasses residues Gln597-Ile-611, while helices α2 and α3 span residues Arg-623-Tyr-640 and Arg-646–Lys-662, respectively. Helices α1 and α3 are coplanar and pack approximately parallel to one another at an angle of $\sim$17°. Helices α1 and α2 pack at an angle of $\sim$55°, making contacts throughout their length. By contrast, the packing interactions between α2 and α3 are limited to only a few residues at their C and N termini, respectively. α1 and α2 are connected by an 11-residue linker that forms a short 3_{10} helix (G2, residues Pro-617–Lys-621). The narrow backbone resonances observed for residues in this region suggest that this linker might be somewhat flexible. Indeed, this is the region of greatest variability in KIX domain sequences and can even accommodate a two-residue deletion (Figure 1A). The linker between helices α2 and α3 is much shorter (about five residues) and adopts a turn-like conformation. The other 3_{10} helix, G1, is near the N terminus and encompasses residues Trp-591–His-594.

The secondary structural elements pack together to enclose an extensive hydrophobic core. The primary core formed by residues Trp-591, Val-595, Leu-599, Leu-603, Met-639, Tyr-640, Ala-643, Tyr-649, and Leu-653 at the junction of helices α1, α2, α3, and G1, is continued along the lengths of the three α helices by residues Leu-607, Ala-610, Ile-611, Tyr-631, Ala-632, Val-635, Leu-652, Ile-657, and Ile-660 (Figure 3C). This primary core is adjacent to a secondary hydrophobic core comprising residues Phe-612, Pro-615, Ala-619, Leu-620 in the α1–α2 linker and G2 helix, and residues Val-604, Val-608, Met-625, and Val-629 on the α1 and α2 helices (Figure 3C). Leu-628 bridges the two hydrophobic cores. Both hydrophobic cores are highly conserved in the known KIX domain sequences (Figure 1A).

The tyrosine residues and the single tryptophan in the hydrophobic core appear from the structure to participate in hydrogen bonding interactions through their side-chain hydroxyl or indole NH functionalities. Thus, the Trp-591 $N^{\varepsilon}H$ forms a hydrogen bond to the Ala-644 carbonyl oxygen, and the $O^{\eta}H$ protons of Tyr-640 and Tyr-649 hydrogen bond to the backbone carbonyl of Val-595 and the side-chain carboxyl of Glu-636, respectively, in the family of structures. An interaction is observed between the aromatic ring of Tyr-640 and the positively charged guanidinium group of Arg-600. This interaction may be important for the stability of the KIX domain, since replacement of Arg-600 by glutamine significantly impairs binding of KIX to pKID (Parker et al., 1996), even though no direct contacts are made between this residue and pKID in the NMR structures. It is interesting that both the arginine and the aromatic residue (Tyr or Phe) are conserved at these positions in all known KIX domain sequences (Figure 1A). Stabilizing interactions between aromatic rings and guanidinium groups have been reported in a number of crystal structures (Flocco and Mowbray, 1994; Mitchell et al., 1994).

Structure of pKID

Upon binding to KIX, residues 121–143 of pKID undergo significant conformational changes, folding into two mutually perpendicular helices, αA and αB. Helix αA extends from residue Asp-120 to Ser-129 while helix αB is initiated at residue Pro-132 or pSer-133 and extends up to Asp-144. Residues Ala-145 and Pro-146 following the helix adopt more extended conformations in the

Table 1. NMR Structure Determination Statistics

NMR Constraints		
KIX	Distance constraints	1067
	Intraresidue	454
	Sequential ($\|i-j\|=1$)	257
	Medium range ($\|i-j\|\leq 4$)	220
	Long-range ($\|i-j\|>4$)	136
	Ambiguous constraints	380
	Torsion angle constraints	27 ϕ and 8 χ^1
pKID	Distance constraints	117
	Intraresidue	63
	Sequential ($\|i-j\|=1$)	30
	Medium range ($\|i-j\|\leq 4$)	24
	Long-range ($\|i-j\|>4$)	0
	Ambiguous constraints	19
	Torsion angle constraints	18 ϕ and 18 ψ
pKID–KIX	Distance constraints	89
	Ambiguous constraints	21
Structure Statistics (16 Structures)		
Violation Statistics		
	NOE violations $>$ 0.1 Å	11.5 $\pm$ 2.3
	Maximum NOE violation	0.3 Å
	Torsion angle constraint violations $>0°$	0.4 $\pm$ 0.5
	Maximum torsion angle violation	5°
Energies		
	Mean constraint violation energy	9.5 $\pm$ 1.1 kcal mol^{-1}
	Mean AMBER energy	-1658 ± 15 kcal mol^{-1}
Mean Deviations from Ideal Covalent Geometry		
	Bond lengths	0.003 Å
	Bond angles	1.3°
PROCHECK Statistics[1]		
	Residues in most favored regions	89.6%
	Residues in allowed regions	9.0%
RMS Deviations from the Average Structure		
KIX	Backbone atoms (N, C^α, C′, O)	
	All residues	0.95 Å
	Helices	0.49 Å
pKID	Backbone atoms (N, C^α, C′, O)	
	All residues	0.95 Å
	Helices	0.86 Å
pKID + KIX	All heavy atoms	1.63 Å
	Backbone atoms (N, C^α, C′, O)	
	All residues	1.10 Å
	Helices	0.82 Å
	Helices (excluding αA of pKID)	0.53 Å

[1] Laskowski et al., 1996.

NMR structures. The αB helix is very well-defined in its interactions and orientation relative to KIX, consistent with the large number of intermolecular NOEs (83) involving residues in this helix. By contrast, the orientation of helix αA relative to αB is not so well-defined in the NMR structures (Figure 3A), although the region is helical in all of the structures. This reflects the paucity of NOEs between helix αA and KIX (only six NOEs, five of which are from Leu-128). Because of the broadness of many of the resonances, relatively few NOEs were observed from residues in the short linker between helices αA and αB. Although the conformation of the backbone in this region is relatively well determined due to the constraints imposed by the adjacent helices and the observed interactions with KIX, the conformation of some of the side-chains cannot be determined with great precision from the NMR data.

Except for contacts between Tyr-134 and Leu-128, direct interactions between αA and αB are minimal. Both helices appear to be primarily stabilized by packing against the surface of KIX, rather than against each other. However, the aromatic ring of Tyr-134 is wedged between the two helices such that it makes van der Waals contact with Leu-128 in helix αA and with Leu-138 in helix αB. These interactions define a small hydrophobic core within pKID.

The pKID-KIX Interface

Residues in the amphipathic helix αB of pKID mediate most of the interactions with KIX. Upon complex formation, pKID and KIX bury about 1200 Å^2 of solvent-accessible surface (~600 Å^2 in each protein). The amphipathic helix αB of pKID and the adjacent C-terminal Ala-145

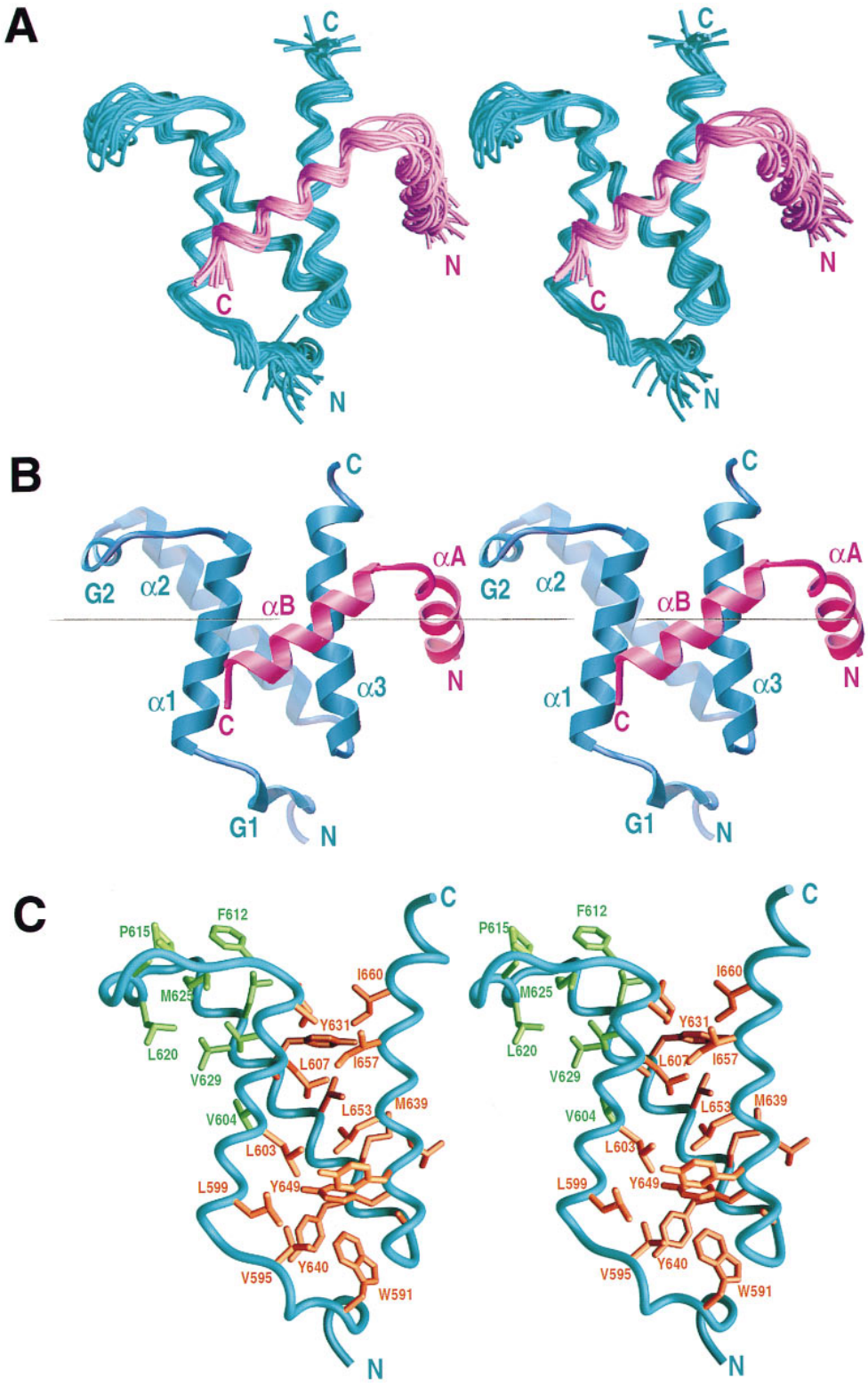

Figure 3. Stereo Views of the Three-Dimensional Structure of the pKID:KIX Complex

(A) C^{α} chain trace of a best-fit superposition of the family of 16 NMR structures. (B) Ribbon diagram of the energy minimized mean structure. (C) Hydrophobic cores of KIX. In (A) and (B), the backbone of KIX is shown in cyan and that of pKID in pink. In (C), the side chains of the primary hydrophobic core are in orange and those of the secondary core in green, and the pKID has been omitted for clarity.

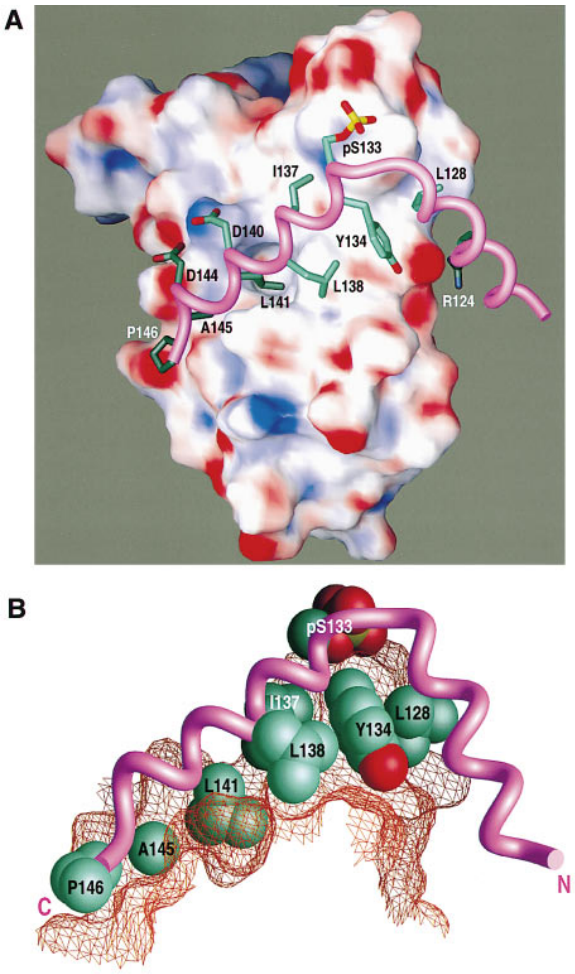

Figure 4. Interactions between KIX and pKID

(A) Molecular surface of KIX. Regions of the surface with electrostatic potentials greater than +15 kT, equal to 0 kT, and less than −15 kT are colored blue, white and red, respectively. Colors are linearly interpolated for the intermediate values. Calculations were performed within GRASP (Nicholls et al., 1991); partial atomic charges were taken from the AMBER 4.1 force field (Pearlman et al., 1995). Residues of pKID that interact with KIX are shown. The backbone of pKID is rendered as a tube (pink).

(B) Hydrophobic interactions between pKID and KIX. The hydrophobic sidechains (CPK spheres) and the backbone (pink) of pKID are shown. The sidechain of pSer-133 is also depicted. The part of the molecular surface of KIX that is within 2.8 Å of the molecular surface of pKID is shown (orange mesh) to emphasize the complementarity between the interacting surfaces.

and Pro-146 account for over 950 Å^2 of this surface, which is predominantly hydrophobic. With the exception of Leu-128, which is buried at the protein–protein interface, and Ile-127, all residues in the αA helix of pKID are either charged or polar and, except for Arg-124, make minimal contact with KIX.

The side chains of residues Leu-599, Leu-603, the aliphatic region of Lys-606, Tyr-650, Leu-653, Ala-654, Ile-657, and Tyr-658, all of which are located in the KIX α1 and α3 helices, form a shallow hydrophobic groove on the surface of the protein (Figure 4). This groove represents the primary docking surface for the nonpolar face, formed by the side chains of Tyr-134, Ile-137, Leu-138, and Leu-141, of the amphipathic αB helix of pKID. Within this groove, there is a deep hydrophobic pocket lined by the side chains of Leu-603, Lys-606, Tyr-650, Leu-653, Ala-654, and Ile-657 of KIX. The side chain of Leu-141 of pKID projects deeply into this pocket, where it is completely buried from solvent (Figure 4). The side chains of Ile-137 and Leu-138 of pKID, located one helical turn from Leu-141, pack against a shallower region of the hydrophobic groove and are relatively more accessible to solvent. Nevertheless, these residues do make extensive van der Waals contacts with Tyr-650, Ala-654, and Ile-657. Tyr-134 of pKID makes van der Waals contacts with the side chains of Glu-655 and Tyr-658 of KIX. The side chains of Tyr-134, Ile-137, Leu-138, and Leu-141 of pKID are thus symmetrically disposed around the methyl group of Ala-654 in the α3 helix of KIX. By virtue of its short side chain, Ala-654 appears to perform a critical function, allowing close approach and optimal packing of the α3 and αB helices in KIX and pKID, respectively. Additional van der Waals contacts are observed between the side chain of Leu-128, located in helix αA of pKID, and Tyr-658 of KIX. These interactions appear to be significant because Leu-128 is highly conserved in the KID region of the various CREB family members (Figure 1B). Finally, further hydrophobic contacts are made between the side chains of Ala-145 and Pro-146, which follow helix αB of pKID, and residues of KIX near the end of the binding groove. Ala-145 interacts primarily with Leu-603 of KIX but also contacts Leu-599, His-602, and Tyr-650. Pro-146 of pKID interacts only with Leu-599 of KIX.

The hydrophobic interactions between the two proteins are supplemented by electrostatic interactions. The side chain of Asp-140, located on the polar face of the αB helix of pKID, contacts the ϵ-amino group of Lys-606 in helix α1 of KIX (Figure 5). This interaction appears to be important for stabilizing the complex because nonconservative substitution of the aspartate residue reduces the transactivation potential of CREB (Gonzalez et al., 1991), and furthermore, an acidic residue is invariant at this position within the CREB family (Figure 1B). A second aspartate side chain, belonging to Asp-144, is located close to both the Lys-606 amino group and the side chain of His-602 of KIX. An acidic residue is conserved at this position in all members of the CREB family with the exception of the Drosophila proteins (Figure 1B). Finally, the guanidinium group of Arg-124 on helix αA of pKID is located near the side chain carboxyl of Glu-655; a basic residue is found at this position in most members of the CREB family.

Role of the Phosphoserine in pKID:KIX Complex Formation

The interaction between CREB and CBP is critically dependent upon phosphorylation of a specific serine residue (Ser-133) in the KID region of CREB. In the NMR structures, pSer-133 is located near the N terminus of the αB helix of pKID. Its phosphate moiety, although not very well-defined in the family of NMR structures due to a lack of restraints, is directed toward the side chains of Tyr-658 and Lys-662 in most of the structures

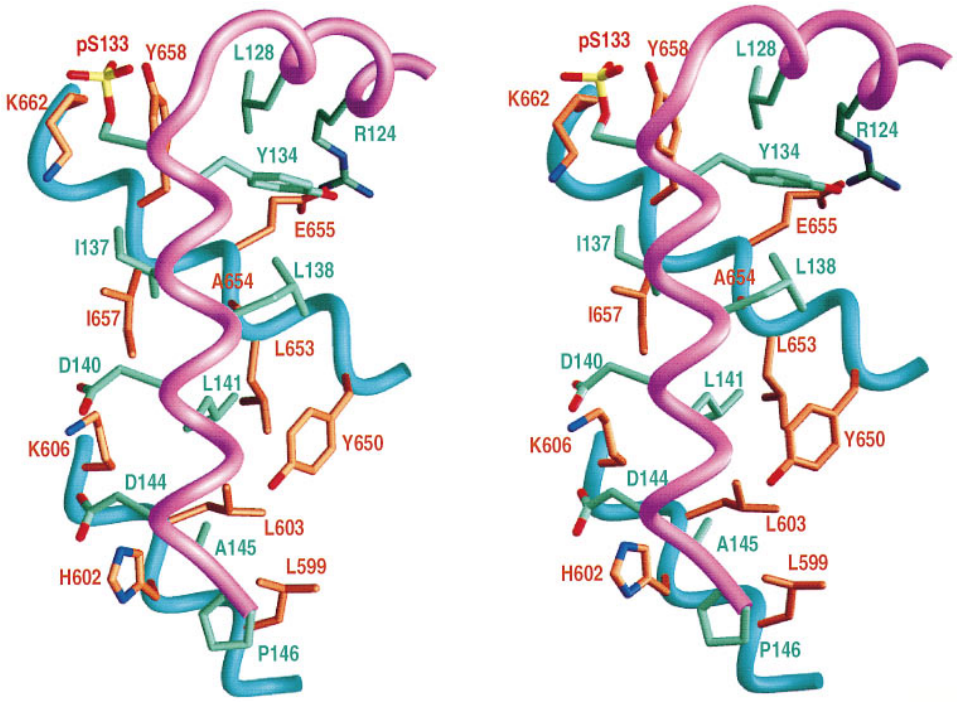

Figure 5. Side Chains in the KIX:pKID Interface

Details of noncovalent interactions between sidechains of pKID (green) and KIX (orange) at the interface. Noninteracting regions have been omitted for clarity.

in the ensemble. In half of the structures, the phosphate approaches to within hydrogen bonding distance of the Tyr-658 hydroxyl proton. In many of the structures, additional or alternative hydrogen bonding interactions are observed between the phosphate group and the pSer backbone amide. Indeed, both of these hydrogen bonds are formed in the mean, energy-minimized structure (Figure 5). Given the uncertainties about the location of the phosphate group in the NMR structures, mutagenesis experiments were performed to probe its interactions with KIX and gain insights into the role phosphorylation plays in facilitating pKID binding. Despite its proximity to the phosphate, substitution of Lys-662 by alanine causes no apparent change in phospho-CREB binding affinity (Figure 6), indicating that electrostatic interactions involving this lysine are not essential for binding. In contrast, mutation of Tyr-658 of KIX to phenylalanine attenuates phospho-CREB binding 3- to 4-fold while mutation to alanine completely abrogates complex formation in vitro (Figure 6). The decreased affinity of Tyr-658-Phe KIX provides compelling evidence that a hydrogen bonding interaction between pSer-133 and the Tyr-658 side chain plays a critical role in stabilization of the pKID:KIX complex. The additional loss of binding competency in the Tyr-658Ala mutant can be attributed to disruption of interfacial hydrophobic contacts between the aromatic ring of residue 658 and residues Leu-128 and Tyr-134 of pKID. We note that interactions between the tyrosine hydroxyl group and phosphate have been observed frequently in protein structures; in fact, a statistical analysis of phosphate binding sites in proteins ranks the propensity of tyrosine to bind phosphate next only to that of arginine (Copley and Barton, 1994).

By virtue of its location near the N terminus of the αB helix, the phosphate group of pSer-133 could also help to stabilize the helical structure formed upon binding of pKID to KIX through favorable electrostatic interactions with the helix macrodipole. In addition, hydrogen bonding interactions with the pSer-133 backbone amide, observed in many of the NMR structures, may play a role

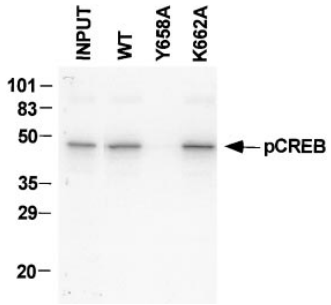

Figure 6. Binding of Ser-133-Phosphorylated CREB to Wild-Type and Mutant KIX Polypeptides

GST pull-down assay of ^{32}P-labeled Ser-133-phosphorylated CREB using GST-KIX resins. INPUT (25% of total ^{32}P-labeled CREB added to individual binding reactions). WT, wild-type KIX polypeptide; Y658A, mutant KIX polypeptide containing a Tyr→Ala substitution at amino acid 658; K662A, mutant KIX polypeptide containing a Lys→Ala substitution at amino acid 662. Equivalent expression of wild-type and mutant GST-KIX polypeptides was confirmed by Coomassie staining (not shown).

in helix capping. However, neither of these interactions appears to be the primary mechanism by which phosphorylation stabilizes the pKID:KIX complex since substitution of Ser-133 by aspartate or glutamate does not lead to constitutive CREB activity (Gonzalez and Montminy, 1989). In addition, phosphorylation of the free KID peptide does not lead to a discernible increase in helix content as determined by NMR experiments. Thus, we conclude that hydrogen bonding interactions between the hydroxyl group of Tyr-658 and the phosphate moiety of pSer-133 play an important role in stabilization of the pKID:KIX complex.

Sequence and Structural Requirements for Kinase-Inducible Activation Domains

The sequences of the kinase-inducible activation domains of CREB family members are highly conserved throughout the region that interacts with the KIX domain of CBP, but show little similarity outside this region (Figure 1B). Many of the conserved amino acids appear to play primarily a structural role, facilitating formation of the amphipathic αB helix and preserving the hydrophobic contacts with the binding groove of KIX. Thus, bulky hydrophobic residues are conserved in all of the key positions on helix αB that contact the hydrophobic surface of the KIX binding groove (Figure 1B). Mutagenesis experiments have shown these residues, Tyr-134, Ile-137, Leu-138, and Leu-141 in rat CREB, to be crucial both for KIX binding and for target gene activation (Parker et al., 1996). Similarly, Leu-128, which makes the sole hydrophobic contact between αA and KIX, is invariant throughout the family. The acidic amino acids on helix αB of pKID (Asp-140 and Asp-144 in rCREB), which contact His-602 and Lys-606 of KIX, are also conserved in most CREB family members (Figure 1B).

Additional amino acids, which appear to play no structural role in formation of the pKID:KIX complex, are highly conserved in the kinase-inducible activation domains (Figure 1B). Like other signal-dependent activation domains, KID appears to mediate target gene induction by associating with cellular kinases, then transmitting the signal via CBP. The function of many of the additional conserved residues is to facilitate phosphorylation of Ser-133 by the cyclic AMP-dependent protein kinase A. Thus, all of the CREB family members contain the invariant sequence Arg-Arg-Pro-Ser-Tyr, which represents a highly preferred sequence for recognition and phosphorylation by protein kinase A (Knighton et al., 1991a, 1991b). Mutations at any of these sites are deleterious (Shih et al., 1996), in accord with their importance for phosphorylation. Clusters of conserved basic residues, which appear to play no role in KIX binding, in both the αA and αB regions may well function in kinase or phosphatase recognition. Indeed, residues extending up to 16 amino acids N-terminal to the serine phosphoacceptor have been shown to stabilize substrate binding to protein kinase A (Knighton et al., 1991b).

The structural differences between the free and KIX-bound forms of KID may reflect, in part, the distinct requirements for binding to protein kinase A and CBP, respectively. The crystal structure of the protein kinase A catalytic subunit bound to an inhibitor peptide reveals that the consensus peptide recognition site (Arg-Arg-X-Ser-Φ, where Φ is a bulky hydrophobic residue and X represents any amino acid) binds in an extended conformation (Knighton et al., 1991b), explaining the absence of substantial secondary structure in the free KID peptide (Parker et al., 1996; this work). By contrast, binding of pKID to KIX requires formation of a C-terminal amphipathic helix (αB) and may be further facilitated by formation of a second helix N-terminal to the phosphorylation site.

Comparison with Other Activation Domains

The structural requirements for physical interactions between transcriptional activators and proteins in the transcriptional apparatus remain enigmatic, in part because transactivation domains share little sequence similarity apart from a general abundance of acidic residues or amino acids such as glutamine or proline. The absence of detectable secondary structure in several activation domains has also strengthened the notion that only limited regions interact with the basal transcription machinery (for review, see Ptashne and Gann, 1997).

The NMR structure of the pKID:KIX complex reveals an important role for an induced amphipathic helix in activator–coactivator recognition. The Ser-133 phosphorylated KID peptide is largely unstructured in the free state; complex formation with KIX triggers a structural transition in which the pKID peptide forms two α helices. This behavior resembles that of the acidic activation domains of p53 and VP16, which undergo transitions from unstructured states to form amphipathic helices upon binding to the attenuator protein MDM2 or to a TATA box-binding protein associated factor (TAF), respectively (Kussie et al., 1996; Uesugi et al., 1997). Further, we note an interesting sequence similarity between the inducible activation domains of the CREB family and the transactivation domain of p53; both domains contain the sequence motif Aro-X-X-Φ-Φ-X-X-Φ, where Aro represents Phe or Tyr. In each case, the aromatic and hydrophobic residues form the face of an amphipathic helix, which mediates binding to the hydrophobic groove of KIX or MDM2, respectively. A key difference between the p53 activation domain and pKID is that constitutive, predominantly hydrophobic interactions are sufficient for complex formation between MDM2 and p53, whereas the hydrophobic contacts made by the amphipathic helix must be supplemented by hydrogen bonding to the phosphoserine in order to stabilize the pKID:KIX complex. These differences are probably related to the presence of a deeper binding cleft in MDM2 than in KIX, and a larger buried surface area (∼1500 Å^2) in the p53:MDM2 complex (Kussie et al., 1996).

KIX Complexes of Other Activation Domains

Several other transcription factors utilize the KIX domain of CBP for their transactivation function (Janknecht and Hunter, 1996). For c-Myb (Dai et al., 1996), Jun (Bannister et al., 1995) and *cubitus interruptus* (Akimaru et al., 1997), the region that interacts with KIX has been mapped. Although the sequences of these domains share little similarity with each other or with CREB, all

contain the motif Glu-Φ-X-X-Φ-Φ (cf. pSer-Φ-X-X-Φ-Φ in pKID) and are predicted to form amphipathic helices. Thus, it is possible that these activation domains may bind in a manner similar to pKID in the hydrophobic groove of KIX. However, a detailed understanding of the interactions involved and why these activation domains are constitutively active, whereas Ser-133Glu KID is not, must await determination of the three-dimensional structures of their complexes with KIX. Thus, the KIX domain could have evolved to recognize diverse partners through a common mechanism, that is, by interacting through its hydrophobic patch. However, the details of the interaction could be different, conferring specificity to the process.

Comparison to Other Phosphopeptide Binding Proteins

Phosphorylation is a common mechanism in many cellular signal transduction processes. Three-dimensional structures of phosphotyrosine-containing peptides bound to SH2 and PTB domains (Waksman et al., 1992; Zhou et al., 1995) have been determined, but despite the importance of serine phosphorylation in signal transduction, little is known about the molecular mechanisms for recognition of phosphoserine-containing peptides by regulatory proteins. The helical KIX domain has an entirely different structure from those of the SH2 and PTB domains, which adopt an $\alpha + \beta$ folding topology. The bound peptide adopts an extended conformation in the SH2 and PTB domain complexes, and the tyrosine phosphoryl group interacts predominantly with basic side chains (Waksman et al., 1992; Zhou et al., 1995). In contrast, the phosphoserine appears to form only a single intermolecular hydrogen bonding contact, to the side chain of Tyr-658, in the pKID:KIX complex; electrostatic interactions with the nearby Lys-662 appear to be unimportant for binding. The phosphotyrosine residue itself appears to make a significant contribution to the overall binding affinity, since free phosphotyrosine is able to bind to SH2 domains (Mayer et al., 1992), and intermolecular interactions are typically limited to a few neighboring residues. In contrast, free phosphoserine exhibits no detectable binding to KIX (Parker et al., 1996); binding to phosphoserine is clearly sequence-specific and depends upon formation of extensive hydrophobic contacts between pKID and the KIX binding groove.

Conclusion

The structure of the complex formed between the KIX domain of CBP and pKID provides insights into the structural basis of phosphoserine recognition in general and into the molecular mechanism by which serine phosphorylation induces the CREB transactivation domain in particular. In common with the p53 and VP16 activation domains (Kussie et al., 1996; Uesugi et al., 1997), binding to the target protein leads to a structural transition from a largely unfolded state to one in which amphipathic helices mediate protein–protein interactions. It is likely that similar folding transitions, leading to amphipathic helix formation in many cases, will play an important role in other transcriptional activation processes, given that activating regions are frequently observed to be unstructured in the absence of their specific protein targets (Ptashne and Gann, 1997). With many transactivation domains predicted to form amphipathic helices, the stage appears to be set to understand issues relating to specificity of these interactions and the mechanisms by which competing factors can influence the processing of signals at the transcriptional level.

Experimental Procedures

Preparation of the KIX Domain

The gene sequence of the KIX domain, corresponding to residues 586–666 of mouse CBP (Chrivia et al., 1993), was amplified using PCR (polymerase chain reaction) and inserted between the NdeI and BamHI restriction sites of the pET-21a(+) expression vector (Novagen). E. coli BL21(DE3) cells harboring the vector were grown at 37°C in LB media. 1 mM isopropyl-1-thio-β-D-galactopyranoside (IPTG) was added for induction of target protein expression when OD_{600nm} was between 0.8 and 1. The cells were harvested 4 hr after addition of IPTG. The cell pellet was resuspended in 50 mM Tris buffer (pH 9.2) containing 0.1 M NaCl, 1 mM phenylmethylsulfonyl fluoride (PMSF), 1 μM leupeptin, and 0.1% Triton X-100. The cells were lyzed by sonication and centrifuged, and the supernatant was loaded onto a Hi-Trap Q column (Pharmacia) for FPLC purification. The protein was eluted using 50 mM Tris buffer (pH 8.0) containing 0.1 M NaCl and purified to homogeneity via reverse phase HPLC using a Vydac C18 column (22 mm × 250 mm). The identity and integrity of the protein was confirmed by mass spectrometry.

Preparation of the KID Domain of CREB

The gene sequence of the KID domain (residues 101–160 plus an initiator methionine) of rat CREB (Gonzalez et al., 1989) was amplified using PCR and subcloned into the pET-24a(+) expression vector (Novagen). E. coli BL21 (DE3) cells were cotransfected with the expression vector and the pUBS520 plasmid (Brinkmann et al., 1989). The cells were grown at 37°C in LB media to OD_{600nm} ~0.6–0.7 before induction with 1 mM IPTG. The cells were harvested 4 hr after addition of IPTG. The cell pellet was resuspended in 50 mM imidazole buffer (pH 7.0) containing 1 mM PMSF, 1 μM leupeptin, and 0.1% Triton X-100. After sonication and centrifugation, the supernatant containing the target protein was loaded onto a Hi-Trap Q column (Pharmacia) for FPLC purification. The target protein was eluted using 50 mM imidazole buffer (pH 5.5) containing 0.1 M NaCl and purified to homogeneity via reverse phase HPLC using a Vydac C18 column (22 mm × 250 mm). The identity and integrity of the protein was confirmed by mass spectrometry.

In Vitro Phosphorylation of KID and Binding Assays

The KID protein was phosphorylated in vitro by incubating 0.07 mM purified protein with 0.35 μM PKA catalytic subunit in the presence of 2 mM ATP, 25 mM Tris-HCl (pH 7.0), 10 mM $MgCl_2$, and 1 mM DTT at 30°C for 1.5 hr. The phosphorylated protein product (pKID) was purified by reverse-phase HPLC, and the extent of phosphorylation (100%) was confirmed by mass spectrometry. Assays for binding of Ser-133 phosphorylated CREB to GST-KIX were performed as described previously (Parker et al., 1996).

Preparation of Uniformly Labeled Proteins

For NMR studies, protein samples uniformly labeled with ^{15}N and/or ^{13}C isotopes were expressed and purified as described above, except cells were grown in M9 minimal media containing ^{15}N-ammonium sulfate and/or $^{13}C_6$-D-glucose, respectively, instead of LB. Uniform labeling was confirmed by mass spectrometry.

pKID:KIX Complex Generation and NMR Sample Preparation

Four forms of the pKID:KIX complex, namely, [^{15}N]-pKID:KIX, [^{15}N,^{13}C]-pKID:KIX, [^{15}N]-KIX:pKID, and [^{15}N,^{13}C]-KIX:pKID were prepared. For each component of the complex, the concentration was

determined from the absorbance at 280 nm, using extinction coefficients ϵ_{280nm}: 12.09 mM^{-1} cm^{-1} for KIX and 1.28 mM^{-1} cm^{-1} for pKID. A 1:1 stoichiometry could thus be determined, but for all complexes prepared, the unlabeled component was kept in slight excess (20%–30%). Complexes were prepared by direct addition of individual components solubilized in 0.6 M guanidinium hydrochloride (Gdn.HCl) containing NMR buffer (20 mM Tris-d_{11} acetate-d_4, pH 5.5, 50 mM NaCl). In the absence of Gdn.HCl, KIX showed a tendency to aggregate while pKID was insoluble. The Gdn.HCl was removed during sample concentration and buffer exchange by ultrafiltration through Centricon membranes with MW 3000 cutoff.

NMR samples in the concentration range 1–1.5 mM were prepared in either 90%H_2O/10%D_2O or 99.996% D_2O (Isotec). All NMR samples were purged with argon, capped, and sealed with parafilm.

NMR Spectroscopy

All NMR experiments were performed on Bruker 500, 600, and 750 MHz spectrometers. Most spectra were recorded at 42°C. NMR data processing and analysis were performed using the Felix 95 software package (Molecular Simulations Inc., San Diego). Sequence-specific resonance assignments for KIX and pKID were made through double- and triple-resonance methods (Bax and Grzesiek, 1993; Clore and Gronenborn, 1994). Backbone resonances for KIX were assigned from three-dimensional (3D) HNCA, HN(CO)CA, HNCO, and HCACO spectra while aliphatic sidechain resonances were assigned using 3D ^{15}N-edited TOCSY, HCCH-TOCSY, and HCCH-COSY spectra. Aromatic sidechain resonances were assigned from 2D and 3D spectra, including (HB)CB(CGCD)HD, (HB)CBCG(CD)HD, (HB)CB(CGCDCE)HE, and (HC)C(C)CH-TOCSY (Yamazaki et al., 1993; Löhr and Rüterjans, 1996). Almost all backbone and sidechain resonances could be assigned in KIX.

Because of the problems of resonance broadening and spectral overlap, NMR spectra for pKID were recorded at both 42°C and 17°C. Backbone resonances were assigned using 3D HNCA, HN(CO)CA, CBCA(CO)NH (both temperatures), and HNCACB (42°C only) spectra. 3D ^{13}C-edited HCCH-TOCSY and ^{15}N-edited TOCSY-HSQC spectra were acquired for side-chain assignments. Several exchange-broadened resonances could only be assigned using sequential NOE connectivities observed in 2D double half-filtered NOESY (τ_m = 120 ms) and TOCSY spectra (Otting and Wüthrich, 1990) and 3D ^{15}N- and ^{13}C-edited NOESY (τ_m = 80 and 70 ms, respectively) spectra. Although backbone resonances could be assigned, only partial assignments could be made for the side chain protons of Arg-130, Arg-131, and Pro-132, and no assignments could be made for pSer-133. A detailed account of the NMR experiments and assignments will be given elsewhere.

Restraint Generation

Interproton distance constraints for KIX were derived from ^{15}N-edited NOESY (τ_m = 100 ms), aliphatic ^{13}C-edited NOESY (τ_m = 50 ms), and aromatic ^{13}C-edited NOESY (τ_m = 25 ms) spectra while those for pKID were derived from ^{15}N-edited NOESY (τ_m = 80 ms), aliphatic ^{13}C-edited NOESY (τ_m = 70 ms), and double half-filtered NOESY (τ_m = 120 ms) spectra. Cross peak intensities were calibrated against known interproton distances in regular structural elements (α helices) or between protons of fixed separation. Distance constraints were assigned upper bounds of 3, 4, and 5 Å; all lower bounds were set to the van der Waals contact distance (1.8 Å). Because of the longer mixing time, the upper bounds for the constraints derived from ^{15}N-edited NOESY (for KIX) and from double half-filtered NOESY (for pKID), were increased by 0.5 Å. Distance constraints derived from ^{15}N-edited NOESY spectra of pKID were assigned loose upper bounds of 3.5 or 5.0 Å. Appropriate pseudo-atom corrections to the upper bounds were applied to constraints involving nonstereospecifically assigned methyl and methylene groups and aromatic ring protons. No explicit hydrogen bonding constraints were imposed.

Intermolecular distance constraints were derived from a 3D ^{13}C(ω_2)-edited,^{13}C(ω_3)-filtered NOESY (τ_m = 120 ms) experiment (Lee et al., 1994). A scaling factor was determined by comparing the intensities of well-resolved peaks with those of the corresponding peaks in the ^{13}C-edited NOESY spectrum acquired for KIX. Upper bounds of 3, 4, and 5.5 Å were assigned on the basis of the scaled intensities.

A total of 27 ϕ and 8 χ_1 torsion angle constraints for KIX were derived from HNHA and constant-time spin-echo difference spectra, respectively (Vuister et al., 1993; Kuboniwa et al., 1994). Backbone torsion angles for 18 residues of pKID were restrained to the ranges $-90°$ to $-30°$ (ϕ) and $-100°$ to 0° (ψ) on the basis of their chemical shifts. These constraints were applied only to residues for which C^α and H^α secondary shifts unequivocally established helical conformations (Spera and Bax, 1991).

Structure Calculations and Analyses

Initial structures were calculated separately for KIX and pKID with intramolecular distance and torsion angle constraints determined for the complex. For KIX, 100 structures were calculated with the program DIANA (Güntert et al., 1991) using the REDAC strategy (Güntert and Wüthrich, 1991). The 60 structures with the lowest target functions ($<$1.1) were refined by simulated annealing (SA) using the AMBER 4.1 suite of programs (Pearlman et al., 1995), with the force field modified to reduce charges to 20%. The 40 structures with the lowest constraint energies were chosen for subsequent docking calculations. A total of 50 structures was calculated for pKID using DIANA, in the manner described for KIX. The 40 structures with the lowest target functions ($<$0.72) were selected directly for docking calculations.

Starting structures for docking were generated within INSIGHTII (Molecular Simulations Inc., San Diego). Pairs of pKID and KIX conformers were selected at random and placed about 50 Å apart. The starting structures were subjected to three cycles of SA with each cycle comprising a heating phase for 4 ps followed by 2 ps of equilibration and 14 ps of slow cooling to 0 K (timestep = 1 fs). Starting at 0 K, the system was heated to 600 K in the first cycle and to 1200 and 300 K, respectively, in the successive cycles. The final values for the force constants for distance and torsion angle restraints were 20 kcal mol^{-1} $Å^{-1}$ and 32 kcal mol^{-1} rad^{-2}, respectively. The force constants were increased linearly starting with one-tenth of their final values during the heating phase of each SA cycle. The force constants for the intermolecular restraints were increased linearly to their final values during the length of the simulation (20 ps) in the first SA cycle. Each cycle of SA was followed by 1000 steps of restrained minimization (rMIN). At the conclusion of the three SA/rMIN cycles, the 16 structures with the lowest constraint violation energies were selected for analysis.

Analysis of the structures was performed using PROCHECK (Laskowski et al., 1996), PROMOTIF (Hutchinson and Thornton, 1996) and in-house programs. The interfacial surface areas were computed using the MSMS program (Sanner et al., 1996). Graphics images were generated using GRASP (Nicholls et al., 1991) or AVS (Upson et al., 1989).

Acknowledgments

We thank Drs. Mark Foster, David Case, Danilo Casimiro, Signe Holmbeck, Xiang Li, and John Chung for valuable discussions and assistance; Dr. Susan Taylor for providing kinase; Martine Reymond and Linda Tennant for technical assistance; Michael Pique for assistance with graphics; and MSI for access to NMR software. This work was supported by grants from the National Institutes of Health (P. E. W. and M. R. M.), the Skaggs Institute for Chemical Biology (P. E. W.), and the Iacocca Foundation (M. R. M. and D. P.). I. R. and G. C. P. A. were supported by the Jane Coffin Childs Foundation and the Leukemia Society of America.

Received September 9, 1997; revised October 29, 1997.

References

Akimaru, H., Chen, Y., Dai, P., Hou, D.-X., Nonaka, M., Smolik, S.M., Armstrong, S., Goodman, R.H., and Ishii, S. (1997). Drosophila CBP is a co-activator of *cubitus interruptus* in *hedgehog* signaling. Nature *386*, 735–738.

Altschul, S.F., Gish, W., Miller, W., Myers, E.W., and Lipman, D.J. (1990). Basic local alignment search tool. J. Mol. Biol. *215*, 403–410.

Arias, J., Alberts, A.S., Bindle, P., Claret, F.X., Smeal, T., Karin, M., Feramisco, J., and Montminy, M. (1994). Activation of cAMP and mitogen responsive genes relies on a common nuclear factor. Nature *370*, 226–229.

Bannister, A.J., and Kouzarides, T. (1996). The CBP co-activator is a histone acetyltransferase. Nature *384*, 641–643.

Bannister, A.J., Oehler, T., Wilhelm, D., Angel, P., and Kouzarides, T. (1995). Stimulation of c-Jun activity by CBP: c-Jun residues Ser63/73 are required for CBP induced stimulation *in vivo* and CBP binding *in vitro*. Oncogene *11*, 2509–2514.

Bax, A., and Grzesiek, S. (1993). Methodological advances in protein NMR. Acc. Chem. Res *26*, 131–138.

Bhattacharya, S., Eckner, R., Grossman, S., Oldread, E., Arany, Z., D'Andrea, A., and Livingston, D.M. (1996). Cooperation of Stat2 and p300/CBP in signaling induced by interferon-α. Nature *383*, 344–347.

Brindle, P., Linke, S., and Montminy, M. (1993). Analysis of a PK-A dependent activator in CREB reveals a new role for the CREM family of repressors. Nature *364*, 821–824.

Brinkmann, U., Mattes, R.E., and Buckel, P. (1989). High-level expression of recombinant genes in *Escherichia coli* is dependent on the availability of the dnaY gene product. Gene *85*, 109–114.

Chakravarti, D., LaMorte, V.J., Nelson, M.C., Nakajima, T., Schulman, I.G., Juguilon, H., Montminy, M., and Evans, R.M. (1996). Role of CBP/P300 in nuclear receptor signaling. Nature *383*, 99–103.

Chrivia, J.C., Kwok, R.P., Lamb, N., Hagiwara, M., Montminy, M., and Goodman, R.H. (1993). Phosphorylated CREB binds specifically to nuclear protein CBP. Nature *365*, 855–859.

Clore, G.M., and Gronenborn, A.M. (1994). Multidimensional heteronuclear Nuclear Magnetic Resonance of proteins. Meth. Enzymol *239*, 349–363.

Copley, R.R., and Barton, G.J. (1994). A structural analysis of phosphate and sulphate binding sites in proteins: estimation of propensities for binding and conservation of phosphate binding sites. J. Mol. Biol. *242*, 321–329.

Dai, P., Akimaru, H., Tanaka, Y., Hou, D.X., Yasukawa, T., Kanei-Ishii, C., Takahashi, T., and Ishii, S. (1996). CBP as a transcriptional coactivator of c-Myb. Genes Dev. *10*, 528–540.

Ferreri, K., Gill, G., and Montminy, M. (1994). The cAMP regulated transcription factor CREB interacts with a component of the TFIID complex. Proc. Natl. Acad. Sci. USA. *91*, 1210–1213.

Flocco, M.M., and Mowbray, S.L. (1994). Planar stacking interactions of arginine and aromatic side-chains in proteins. J. Mol. Biol. *235*, 709–717.

Gonzalez, G.A., and Montminy, M.R. (1989). Cyclic AMP stimulates somatostatin gene transcription by phosphorylation of CREB at serine-133. Cell *59*, 675–680.

Gonzalez, G.A., Yamamoto, K.K., Fischer, W.H., Karr, D., Menzel, P., Biggs, W., III, Vale, W.W., and Montminy, M.R. (1989). A cluster of phosphorylation sites on the cyclic AMP-regulated nuclear factor CREB predicted by its sequence. Nature *337*, 749–752.

Gonzalez, G.A., Menzel, P., Leonard, J., Fischer, W.H., and Montminy, M. (1991). Characterization of motifs which are critical for activity of the cyclic AMP-responsive transcription factor CREB. Mol. Cell. Biol. *11*, 1306–1312.

Güntert, P., and Wüthrich, K. (1991). Improved efficiency of protein structure calculations from NMR data using the program DIANA with redundant dihedral angle constraints. J. Biomol. NMR *1*, 447–456.

Güntert, P., Braun, W., and Wüthrich, K. (1991). Efficient computation of three-dimensional protein structures in solution from nuclear magnetic resonance data using the program DIANA and the supporting programs CALIBA, HABAS and GLOMSA. J. Mol. Biol. *217*, 517–530.

Hagiwara, M., Alberts, A., Brindle, P., Meinkoth, J., Feramisco, J., Deng, T., Karin, M., Shenolikar, S., and Montminy, M. (1992). Transcriptional attenuation following cAMP induction requires PP-1-mediated dephosphorylation of CREB. Cell *70*, 105–113.

Holm, L., and Sander, C. (1994). The FSSP database of structurally aligned protein fold families. Nucl. Acids Res. *22*, 3600–3609.

Hutchinson, E.G., and Thornton, J.M. (1996). PROMOTIF-A program to identify and analyze structural motifs in proteins. Protein Sci. *5*, 212–220.

Janknecht, R., and Hunter, T. (1996). Transcriptional control: versatile molecular glue. Curr. Biol. *6*, 951–954.

Janknecht, R., and Nordheim, A. (1994). Regulation of the *c-fos* promoter by the ternary complex factor Sap-1a and its coactivator CBP. Oncogene *12*, 1961–1969.

Kamei, Y., Xu, L., Heinzel, T., Torchia, J., Kurokawa, R., Gloss, B., Lin, S.-C., Heyman, R.A., Rose, D.W., Glass, C.K., and Rosenfeld, M.G. (1996). A CBP integrator complex mediates transcriptional activation and AP-1 inhibition by nuclear receptors. Cell *85*, 403–414.

Kee, B., Arias, J., and Montminy, M. (1996). Adaptor mediated recruitment of RNA polymerase II to a signal dependent activator. J. Biol. Chem. *271*, 2373–2375.

Knighton, D.R., Zheng, J., Eyck, L.F.T., Ashford, V.A., Xuong, N.-H., Taylor, S.S., and Sowadski, J.M. (1991a). Crystal structure of the catalytic subunit of cyclic adenosine monophosphate-dependent protein kinase. Science *253*, 407–420.

Knighton, D.R., Zheng, J., Ten Eyck, L.F., Xuong, N.-H., Taylor, S.S., and Sowadski, J.M. (1991b). Structure of a peptide inhibitor bound to the catalytic subunit of cyclic adenosine monophosphate-dependent protein kinase. Science *253*, 414–420.

Kuboniwa, H., Grzesiek, S., Delaglio, F., and Bax, A. (1994). Measurement of H^N-H^α J couplings in calcium-free calmodulin using new 2D and 3D water-flip-back methods. J. Biomol. NMR *4*, 871–878.

Kussie, P.H., Gorina, S., Marechal, V., Elenbaas, B., Moreau, J., Levine, A.J., and Pavletich, N.P. (1996). Structure of the MDM2 oncoprotein bound to the p53 tumor suppressor transactivation domain. Science *274*, 948–953.

Kwok, R.P.S., Lundblad, J.R., Chrivia, J.C., Richards, J.P., Bächinger, H.P., Brennan, R.G., Roberts, S.G.E., Green, M.R., and Goodman, R.H. (1994). Nuclear protein CBP is a coactivator for the transcription factor CREB. Nature *370*, 223–226.

Kwok, R.P.S., Laurance, M.E., Lundblad, J.R., Goldman, P.S., Shih, H., Connor, L.M., Marriott, S.J., and Goodman, R.H. (1996). Control of cAMP-regulated enhancers by the viral transactivator Tax through CREB and the co-activator CBP. Nature *380*, 642–646.

Laskowski, R.A., Rullmann, J.A.C., MacArthur, M.W., Kaptein, R., and Thornton, J.M. (1996). AQUA and PROCHECK-NMR: programs for checking the quality of protein structures solved by NMR J. Biomol. NMR *8*, 477–486.

Lee, W., Revington, M.J., Arrowsmith, C., and Kay, L.E. (1994). A pulsed field gradient isotope-filtered 3D ^{13}C HMQC-NOESY experiment for extracting intermolecular NOE contacts in molecular complexes. FEBS Lett. *350*, 87–90.

Löhr, F., and Rüterjans, H. (1996). Novel pulse sequences for the resonance assignment of aromatic side chains in ^{13}C-labeled proteins. J. Magn. Reson. Series B *112*, 259–268.

Mayer, B.J., Jackson, P.K., Van Etten, R.A., and Baltimore, D. (1992). Point mutations in the *abl* SH2 domain coordinately impair phosphotyrosine binding in vitro and transforming activity in vivo. Mol. Cell. Biol. *12*, 609–618.

Mitchell, J.B.O., Nandi, C.L., McDonald, I.K., Thornton, J.M., and Price, S.L. (1994). Amino/aromatic interactions in proteins: is the evidence stacked against hydrogen bonding? J. Mol. Biol. *239*, 315–331.

Nakajima, T., Uchida, C., Anderson, S., Parvin, J., and Montminy, M. (1997a). RNA helicase A mediates association of CBP with RNA polymerase II. Cell *90*, 1107–1112.

Nakajima, T., Uchida, C., Anderson, S., Parvin, J., and Montminy, M. (1997b). Analysis of a cAMP responsive activator reveals a two-component mechanism for transcriptional induction via signal-dependent factors. Genes Dev. *11*, 738–747.

Nicholls, A., Sharp, K.A., and Honig, B. (1991). Protein folding and association: insights from the interfacial and thermodynamic properties of hydrocarbons. Proteins *11*, 281–296.

Ogryzko, V.V., Schiltz, R.L., Russanova, V., Howard, B.H., and Nakatani, Y. (1996). The transcriptional coactivators p300 and CBP are histone acetyltransferases. Cell *87*, 953–959.

Otting, G., and Wüthrich, K. (1990). Heteronuclear filters in two-dimensional [^{1}H,^{1}H]-NMR spectroscopy: combined use with isotope

labelling for studies of macromolecular conformation and intermolecular interactions. Quart. Rev. Biophys. *23*, 39–96.

Parker, D., Ferreri, K., Nakajima, T., LaMorte, V.J., Evans, R., Koerber, S.C., Hoeger, C., and Montminy, M. (1996). Phosphorylation of CREB at Ser133 induces complex formation with CPB via a direct mechanism. Mol. Cell. Biol. *16*, 694–703.

Pearlman, D.A., Case, D.A., Caldwell, J.W., Ross, W.S., Cheatham, T.E., III, Ferguson, D.M., Seibel, G.L., Singh, U.C., Weiner, P.K., and Kollman, P.A. (1995). AMBER 4.1. (San Francisco: University of California).

Ptashne, M., and Gann, A. (1997). Transcriptional activation by recruitment. Nature *386*, 569–577.

Sanner, M.F., Olson, A.J., and Sphener, J.-C. (1996). Reduced surface: an efficient way to compute molecular surfaces. Biopolymers *38*, 305–320.

Shih, H.M., Goldman, P.S., DeMaggio, A.J., Hollenberg, S.M., Goodman, R.H., and Hoekstra, M.F. (1996). A positive genetic selection for disrupting protein–protein interactions: identification of CREB mutations that prevent association with the coactivator CBP. Proc. Natl. Acad. Sci. USA. *93*, 13896–13901.

Spera, S., and Bax, A. (1991). Empirical correlation between protein backbone conformation and C^{α} and $C\beta^{13}C$ nuclear magnetic resonance chemical shifts. J. Am. Chem. Soc. *113.*, 5490–5492.

Uesugi, M., Nyanguile, O., Lu, H., Levine, A.J., and Verdine, G.L. (1997). Induced α helix in the VP16 activation domain upon binding to a human TAF. Science. *277*, 1310–1313.

Upson, C., Faulhaber, T., Jr., Kamins, D., Laidlaw, D., Vroom, J., Gurwitz, R., and van Dam, A. (1989). The application visualization system: a computational environment for scientific visualization. IEEE Comp. Graph. Appl. *9*, 30–42.

Vuister, G.W., Wang, A.C., and Bax, A. (1993). Measurement of three-bond nitrogen-carbon *J* couplings in proteins uniformly enriched in ^{15}N and ^{13}C. J. Am. Chem. Soc. *115*, 5334–5335.

Waksman, G., Kominos, D., Robertson, S.C., Pant, N., Baltimore, D., Birge, R.B., Cowburn, D., Hanafusa, H., Mayer, B.J., Overduin, M., Resh, M.D., Rios, C.B., Silverman, L., and Kuriyan, J. (1992). Crystal structure of the phosphotyrosine recognition domain SH2 of v-src complexed with tyrosine-phosphorylated peptides. Nature. *358*, 646–653.

Yamazaki, T., Forman-Kay, J.D., and Kay, L.E. (1993). Two-dimensional NMR experiments for correlating $^{13}C\beta$ and $^{1}H\delta/\epsilon$ chemical shifts of aromatic residues in ^{13}C-labeled proteins via scalar couplings. J. Am. Chem. Soc. *115*, 11054–11055.

Zhou, M.-M., Ravichandran, K.S., Olejniczak, E.T., Petros, A.M., Meadows, R.P., Sattler, M., Harlan, J.E., Wade, W.S., Burakoff, S.J., and Fesik, S.W. (1995). Structure and ligand recognition of the phosphotyrosine binding domain of Shc. Nature *378*, 584–592.

Brookhaven Protein Data Bank Accession Number

The accession number for the coordinates of the structures reported in this paper is 1kdx.